Size and interface effects on ferromagnetic and antiferromagnetic transition temperatures

X. Y. Lang, W. T. Zheng, and Q. Jiang*

Key Laboratory of Automobile Materials (Jilin University), Ministry of Education, and Department of Materials Science and Engineering, Jilin University, Changchun 130025, China

(Received 27 February 2006; revised manuscript received 8 May 2006; published 30 June 2006)

A simple and unified model, which is based on the energy-equilibrium criterion between the spin-spin exchange interactions and the thermal vibration energy of atoms at the transition temperature and a size-dependent Debye temperature function $\Theta_D(D)$, has been established for the size, dimension, and interface effects on the Curie temperature $T_c(D)$ and the Néel temperature $T_N(D)$ of low-dimensionally ferromagnetic and antiferromagnetic nanocrystals, where D denotes the diameter of nanoparticles and nanorods or the thickness of thin films. In terms of this model, $T_c(D)$ and $T_N(D)$ functions are predicted to increase or decrease with dropping D, depending on the interaction strength at the film/substrate interface when the interface exists. The predicted results are consistent with available experimental measurements for Fe, Co, Ni, Gd, Ho, Co_1Ni_1, Co_1Ni_3, Co_1Ni_9, Fe_3O_4, $MnFe_2O_4$, CoO, NiO, and CuO low-dimensional nanocrystals.

DOI: 10.1103/PhysRevB.73.224444 PACS number(s): 75.30.Kz, 75.50.Cc, 75.50.Ee, 75.70.−i

I. INTRODUCTION

Fascinating physicochemical properties of low-dimensional nanocrystals (nanoparticles, nanorods, and thin films) and wide possibilities of using these properties in practice have attracted great interest. The current progress in nanotechnologies has made the fabrication of individual nanocrystals possible, which in turn provides an opportunity to study the basic properties of nanocrystals. As an example of the broad class of cooperative phenomena, ferromagnetics (FM) and antiferromagnetics (AFM) of nanocrystals differ from that of the corresponding bulk ones, which is attributed to the different degrees of ordering to occur near surfaces or interface of nanocrystals, leading to an intrinsic size dependence.[1]

The Curie temperature T_c and the Néel temperature T_N are the most important properties to characterize FM and AFM phase stability, respectively. Size dependences of T_c and T_N have been considered intensively in experiments[2–34] and theories[35–40] due to their scientific and industrial importance. It has been found that, as the size of nanocrystals D decreases, $T_c(D)$ of thin FM films epitaxially grown on inert substrates decreases in many systems of Fe/SiO (Ref. 2), Fe/Ag(001) (Ref. 3), Fe/Au(100) (Ref. 4), Fe/Pd(100) (Ref. 5), Fe/Ag(111) (Ref. 6), Fe/Ag(100) (Ref. 7), Co/Cu(100) (Refs. 8,10), Co/Cu(111) (Ref. 10), Co/Cu(001) (Refs. 9,11), Ni/Cu(111) (Refs. 10,12), Ni/Cu(100) (Ref. 10), Ni/Cu(001) (Refs. 9,11), Ni/W(110) (Ref. 13), Co_1Ni_1/Cu(100) (Ref. 10), Co_1Ni_3/Cu(100) (Ref. 10), Co_1Ni_9/Cu(100) (Ref. 10), Gd/W(110) (Ref. 14), Gd/W (Ref. 15), Nb/Gd (Ref. 16), and Gd/Y(0001) (Ref. 17). This case is also present in other low-dimensional nanocrystals, such as Ni nanorods[18,19] and nanoparticles,[19,20,39] Gd,[21] Fe_3O_4,[39] and $MnFe_2O_4$[22] nanoparticles. Besides, $T_N(D)$ values of the low-dimensional AFM nanocrystals, such as Ho (Ref. 23), CoO (Refs. 26,27), NiO (Refs. 28,29) thin films, and CuO nanoparticles[30–33] and nanorods[33] decrease with decreasing of D. The $T_N(D)$ function of CoO thin films supported by Fe_3O_4 and NiO substrates, however, increases as D decreases.[28,34]

Based on the aforementioned experimental evidence, numerous models have been proposed to understand the underlying mechanisms for the $T_c(D)$ and $T_N(D)$ functions of thin films. Among them, the pioneering theoretical work of Fisher and his co-workers strongly influences our general understanding,[35] which predicts that $T_c(D)$ will shift to a lower temperature than that of the bulk $T_c(\infty)$ when the spin-spin correlation length (SSCL) ξ exceeds the film thickness. For thin films, the SSCL mechanism has given rise to a step function for $T_c(D)$ with two adjustable parameters: One is ξ and the other is the exponent term λ.[35,36] When $D > \xi$,

$$T_c(D)/T_c(\infty) = 1 - [(\xi + r_0)/(2D)]^{\lambda}, \tag{1a}$$

while when $D < \xi$,

$$T_c(D)/T_c(\infty) = (D - r_0)/(2\xi), \tag{1b}$$

where r_0 denotes thickness of a monolayer.

Since nanoparticles have different characteristics of $T_c(D)$ functions from that of thin films, further unified models are considered to suit these new cases. In light of the effect of the breaking of exchange bonds, the $T_c(D)$ function of nanoparticles has been proposed,[37]

$$T_c(D)/T_c(\infty) = 1 - (3\Delta L)/(2D), \tag{2}$$

where ΔL is the thickness of surface layer of nanoparticles, which characterizes the influence of the surface layer on the $T_c(D)$ function of nanoparticles. However, when this model is utilized to fit experiment data of the $T_c(D)$ function of Fe_3O_4 nanoparticles, a constant ΔL cannot satisfactorily describe this case in the full size range of nanosize.[37]

Since the dimension of nanocrystals the d significantly affects the $T_c(D)$ function, while Eqs. (1) and (2) consider, respectively, the cases of $d=2$ for thin films and $d=0$ for particles, they exhibit different forms due to this reason. Recently, Sun has established a unified model to consider the dimension effect on $T_c(D)$ by incorporating the bond order-length-strength correlation mechanism into the Ising premise (Ref. 39),

$$T_c(D)/T_c(\infty) = 1 + \sum_{i\leqslant 3} \gamma_i (z_{ib} q_i^{-w} - 1), \quad (3)$$

where $q_i = h_i/h = 2/\{1+\exp[(12-z_i)/(8z_i)]\}$ shows a coordination number (CN) dependent reduction of atomic diameter (h), $z_{ib} = z_i/z_b$ with z_i and z_b being the coordinates with and without CN imperfection, respectively, and $\gamma_i = \tau h q_i/D$ is the portion of the atoms in the ith atomic layer from the surface compared to the total number of atoms of the entire solid, and $\tau = 1, 2, 3$ correspond to thin films, nanorods, and nanoparticles, respectively. The power index w is an indicator for the bond nature.[39] When $w \approx 1$, $T_c(D)$ functions of free nanocrystals with different dimensions are predicted with good correspondence of the experimental results whereas D decreases, $T_c(D)$ drops.[39]

Since there is an adjustable parameter in Eq. (3), further efforts are made to develop a model without a free parameter. Based on the size-dependent cohesive energy function, a model for the $T_c(D)$ of thin films has given as (Ref. 38),

$$T_c(D)/T_c(\infty) = \{1 - 1/[2D/(ch) - 1]\} \times \exp\{[-2S_b/(3R)]/[2D/(ch) - 1]\}, \quad (4)$$

where c is the normalized surface or interface area, S_b is the bulk evaporation entropy of crystals, and R is the gas constant. Equation (4) has presented a qualitative explanation for a drop of the $T_c(D)$ function of nanocrystals with decreasing of D.

However, both Eqs. (3) and (4) have neglected the film/substrate interface effect on $T_c(D)$, which could lead to an increase of the $T_c(D)$ function as D is reduced.

Since each aforementioned model only partially corresponds to experimental results well, and dimension and interface effects on the above functions in the models are not emphasized,[35–38,40] thus, an improved model reflecting all effects, especially the interface effect on $T_c(D)$ and $T_N(D)$ functions, is needed.

In this contribution, the size, dimension, and interface effects on the order temperatures of $T_c(D)$ and $T_N(D)$ functions have been established to minimize the number of parameters needed and to fit the maximum number of experimental results of magnetic nanoparticles, nanorods, and thin films that can be found in the literature, which enables us to reproduce the measured results of low-dimensional FM and AFM nanocrystals of Fe, Co, Ni, Gd, Ho, Co_1Ni_1, Co_1Ni_3, Co_1Ni_9, Fe_3O_4, $MnFe_2O_4$, CoO, NiO, and CuO with a unified form.

II. MODEL

In magnetic materials, the spins are coupled through the strong, short-range exchange interactions, and the long-range magnetic dipolar interactions. It is well known that near T_c, there exist two opposite forces: the ordering force due to an exchange interaction of the magnetic moments, and the disordering force of the lattice thermal vibrations. Based on the mean-field approximation (Ref. 36),

$$k_B T_c(\infty) = E_{exc}(\infty), \quad (5)$$

where k_B is the Boltzmann constant and E_{exc} is the spin-spin exchange interaction energy.

The average thermal vibrational energy is related to T by an equipartition relation of $m(2\pi\upsilon_E)^2\sigma^2(T) = k_B T$,[41] where m is the atomic mass, υ_E is the Einstein frequency, and σ is the root-mean-square (rms) thermal average amplitude of atomic vibration. In terms of this relationship and Eq. (5), at $T_c(\infty)$, the thermal vibration of atoms will destroy the ordering due to the exchange interaction of nearest-neighbor atoms with $\sigma^2[T_c(\infty)] = k_B T_c(\infty)/[m(2\pi\upsilon_E)^2] = E_{exc}(\infty)/[m(2\pi\upsilon_E)^2]$. Similarly, based on Lindemann's basic assumption that melting occurs when σ reaches a fraction of atomic diameter f at $T_m(\infty)$, $\sigma^2[T_m(\infty)] = k_B T_m(\infty)/[m(2\pi\upsilon_E)^2] = (fh)^2$ and $\Theta_D(\infty) = f[T_m(\infty)/(mh^2)]^{1/2}$ (Ref. 41). In terms of above three relationships and an assumption that $E_{exc}(\infty)/(2\pi\upsilon_E f^2)^2 = K$ with K being a material constant, it reads,

$$T_c(\infty) \propto \Theta_D^2(\infty). \quad (6)$$

If FM and AFM nanocrystals have the same crystal structure of the corresponding bulk, Eq. (6) can be extended to nanometer size, $T_c(D) \propto \Theta_D^2(D)$. Combining this relationship with Eq. (6) leads to,

$$T_c(D)/T_c(\infty) = \Theta_D^2(D)/\Theta_D^2(\infty). \quad (7)$$

$\Theta_D(D)$ function has been deduced by combining Lindemann's criterion for melting and a related model for size-dependent melting, (Refs. 42,43)

$$\Theta_D^2(D)/\Theta_D^2(\infty) = \exp[-(\alpha - 1)/(D/D_0 - 1)], \quad (8)$$

where $\alpha = \sigma_s^2(D)/\sigma_v^2(D)$ with the subscript s and v denoting the surface atoms and the interior atoms of nanocrystals. D_0 denotes a critical size at which all atoms of a low-dimensional nanocrystal are located on its surface, which depends on dimension d and h through, (Refs. 38,44),

$$D_0 = 2(3 - d)h, \quad (9)$$

where $d = 0$ for particles, $d = 1$ for nanorods, and $d = 2$ for thin films.

In terms of Eqs. (5), (7), and (8), $T_c(D)$ and $E_{exc}(D)$ functions can be expressed as $T_c(D)/T_c(\infty) = E_{exc}(D)/E_{exc}(\infty) = \exp[-(\alpha-1)/(D/D_0-1)]$. The same case should occur for $T_N(D)/T_N(\infty)$ function. Thus,

$$T_c(D)/T_c(\infty) = T_N(D)/T_N(\infty) = \exp[-(\alpha - 1)/(D/D_0 - 1)]. \quad (10)$$

In Eq. (10), a unique unknown material parameter is α, which is a function of materials and also a function of the situation of the surface and interface. For metallic or compound crystals with free surfaces, α is determined by, (Refs. 42 and 43)

$$\alpha_s = 1 + [2S_{vib}(\infty)/(3R)], \quad (11)$$

where subscript s denotes the surface. Although the overall melting entropy S_m consists, at least, of three contributions: positional S_{pos}, vibrational S_{vib}, and electronic component S_{el}, $S_{vib}(\infty)$ is the essential contribution to $S_m(\infty)$ for metals because the contributions of the other terms of S_{pos} and S_{el} on $S_m(\infty)$ are small. Thus, for metallic elements, (Refs. 42,43),

$$S_{vib}(\infty) \approx S_m(\infty). \quad (12)$$

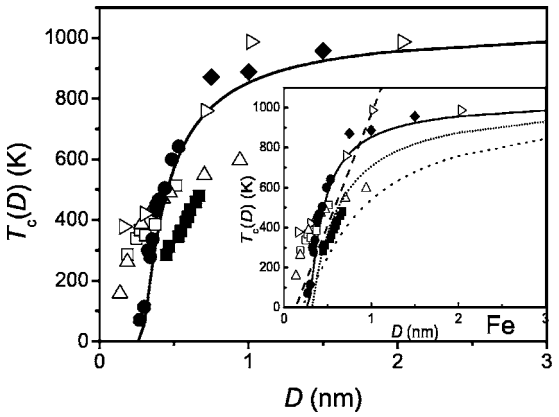

FIG. 1. Comparisons of $T_c(D)$ function between the model prediction in terms of Eq. (14) (solid lines) and the available experimental measurements for Fe/substrate thin films, where the parameters $D_0=(2h)/2=h=0.2483$ nm in terms of Eq. (9) with $d=2$, and $\alpha_i=1.612$ according to Eq. (13) with $J_s\approx J_i$, $J_{\text{sub}}\approx 0$ (Ref. 40) and $\alpha_s=1.612$ in terms of Eq. (11). Other parameters used for calculations are listed in Table I. The symbols ◆ (Ref. 2), ▷ (Ref. 3), ■ (Ref. 4), △ (Ref. 5), ● (Ref. 6), and ■ (Ref. 7) denote the experimental results of Fe/SiO, Fe/Ag(001), Fe/Au(100), Fe/Pd(100), Fe/Ag(111), and Fe/Ag(100) epitaxial films, respectively. Inset: the dashed, short dotted, dotted, and solid lines, respectively, denote the predictions of Eqs. (1b), (3), (4), and (14). The parameters employed in the calculations are listed as: $\xi=0.447$ nm in Eq. (1b) (Ref. 36), the original parameters in Eq. (3) have been cited from the original Ref. 39 with $q_i=0.8756$, 0.9376, 0.9688, $z_{\text{ib}}=1/3$, 1/2, 2/3 with $z_i=4$, 6, 8, and $z_b=12$ for $i=1$, 2, 3, respectively, which is the same for Figs. 2–7, and $c=1/2$ and $S_b=111.52\ J\cdot g\text{-atom}^{-1}\cdot\text{K}^{-1}$ in Eq. (4) (Ref. 38).

When FM or AFM as epitaxially grown film is deposited on a substrate, the effect of such an epitaxial film/substrate interface on α must be considered since the atomic vibration at interface differs from that at a free surface. Based on the Ising model, the simplest case is that only the surface and interface coupling constants (J_s and J_i) differ from the rest,[40] where the subscript i denotes interface. For the sake of simplicity, the effect induced by the exchange interface thickness is neglected while $J_i=J_s+J_{\text{sub}}$ is assumed as a first approximation with the subscript sub denoting the substrate. Thus, $\alpha_i=\sigma_i^2(D)/\sigma_v^2(D)=\alpha_s\sigma_i^2(D)/\sigma_s^2(D)$ in light of the definition of α where $\alpha_s=\sigma_s^2(D)/\sigma_v^2(D)$. Since the magnitude of the exchange interaction is proportional to the bond strength[39,45,46] while the bond strength is reversely proportional to σ^2,[44] $\sigma^2(D)\propto 1/J$. Thus, $\sigma_s^2(D)\propto 1/J_s$ and $\sigma_i^2(D)\propto 1/J_i$. As a result, $\sigma_i^2(D)/\sigma_s^2(D)=J_s/J_i$, or

$$\alpha_i=\alpha_s J_s/J_i. \tag{13}$$

If the effects induced by the surface and interface on $T_c(D)$ and $T_N(D)$ are additive, based on Eq. (10), one can obtain,

$$T_c(D)/T_c(\infty)=T_N(D)/T_N(\infty)=\{\exp[-(\alpha_s-1)/(D/D_0-1)]+\exp[-(\alpha_i-1)/(D/D_0-1)]\}/2. \tag{14}$$

Note that Eq. (14) is only used for the case of thin films while the side surface is neglected since the side surfaces have a small percentage of the total surface in comparison with that of the up surface and bottom interface of thin films. For nanoparticles and nanorods, the contribution of substrates on the order temperatures is neglected since the corresponding interface has only a small percentage of the total surface. In this case, Eq. (10) is directly used. In the following, although $T_c(D)$ and $T_N(D)$ functions are denoted as Eq. (14), when the considered systems are nanoparticles and nanorods, $\alpha_s=\alpha_i$, and thus Eq. (14)=Eq. (10).

III. RESULTS AND DISCUSSION

Figure 1 compares the model prediction of the $T_c(D)$ function in terms of Eq. (14) with available experimental measurements for Fe thin films deposited on inert substrates where the parameters employed in the calculations are listed in Table I. Other models in terms of Eqs. (1), (3), and (4) are also shown in the inset of the figure. Note that, the curve of Eq. (2) is not included in this inset since it corresponds to only nanoparticles.

For epitaxial FM film on an inert substrate with a small lattice mismatch, exchange interaction between them is assumed to be absent since it is assumed that the surface and the film/substrate interface are magnetically similar.[23,40] Thus, $\alpha_i=\alpha_s$ in terms of Eq. (13) with $J_i=J_s$ and $J_{\text{sub}}=0$. On the other side, for this kind of epitaxial films, the interaction strength at the film/substrate interface is comparable with the inner one,[38] which results in the disappearance of one of the two surfaces of films. Thus, the critical size of the epitaxial films is $D_0/2$.[44]

As shown in Fig. 1 and its inset for Fe thin films epitaxially grown on silicon oxide glass,[2] or inert metallic substrates of Ag(001) (Ref. 3), Au(100) (Ref. 4), Pd(100) (Ref.

TABLE I. The parameters employed in the calculations of Eq. (14) about the FM materials. $T_c(\infty)$ is in K, $S_m(\infty)$ in $J\cdot g\text{-atom}^{-1}\cdot\text{K}^{-1}$, and h is in nm.

	$T_c(\infty)$	$S_m(\infty)$[a]	h(nm)[d]
Fe	1043 (Ref. 38)	7.628	0.2483
Co	1404 (Ref. 38)	9.157	0.2497
Ni	630 (Ref. 38)	10.12	0.2492
Gd	289 (Ref. 38)	6.341	0.3575
CoNi	1018 (Ref. 38)	9.638[b]	0.2495
Co_1Ni_3	824.3 (Ref. 38)	9.879[b]	0.2493
Co_1Ni_9	708.3 (Ref. 38)	10.02[b]	0.2493
Fe_3O_4	860 (Ref. 38)	10.55	0.2220
$MnFe_2O_4$	573 (Ref. 22)	10.55[c]	0.2223

[a]The values of $S_m(\infty)$ refer to Ref. 51.
[b]$S_{m,\text{Co}_1\text{Ni}_n}(\infty)=[S_{m,\text{Co}}(\infty)+nS_{m,\text{Ni}}(\infty)]/(n+1)$ as a first approximation, where n denotes the number of Ni atoms in the compounds.
[c]Since no experimental data of $S_{m,\text{MnFe}_2\text{O}_4}(\infty)$ or $S_{\text{vib},\text{MnFe}_2\text{O}_4}(\infty)$ are in hand, $S_{m,\text{MnFe}_2\text{O}_4}(\infty)$ is approximately equal to $S_{m,\text{Fe}_3\text{O}_4}(\infty)$.
[d]The values of h refer to Ref. 51 for elements and Refs. 38 and 39 or compounds, respectively.

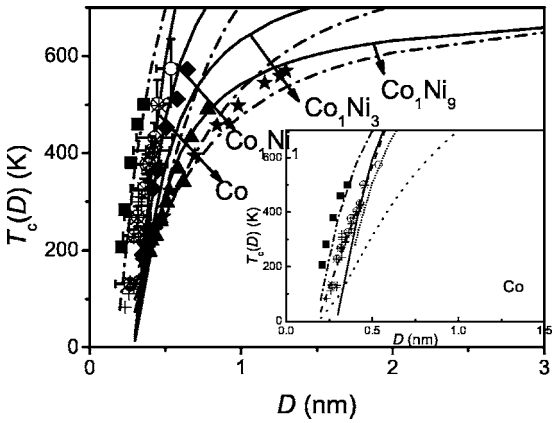

FIG. 2. Comparisons of $T_c(D)$ function between the model prediction in terms of Eqs. (14) (solid lines) and (15) (dash dotted lines) and the available experimental evidences for Co, Co_1Ni_1, Co_1Ni_3, and Co_1Ni_9/substrate epitaxial thin films, where the parameters in Eq. (14) $D_0=(2h)/2=h=0.2497$, 0.2495, 0.2493, and 0.2493 nm in terms of Eq. (9) with $d=2$, and $\alpha_i=1.734$, 1.773, 1.792, and 1.803 according to Eq. (13) with $J_s \approx J_i$, $J_{\text{sub}} \approx 0$ and $\alpha_s=1.734$, 1.773, 1.792, and 1.803 in terms of Eq. (11), respectively. Other parameters used for calculations are listed in Table I. The parameters used in Eq. (15) are $D'=0.195$, 0.150, 0.129 nm, $\xi_0=0.488$, 0.570, 0.518 nm, and $\lambda=1.66$, 1.49, 1.39 for Co_1Ni_1, Co_1Ni_3, and Co_1Ni_9, respectively (Ref. 10). The symbols ○ (Ref. 8), ∗ (Ref. 9 and 10), ■ (Ref. 10), + (Ref. 11) denote the experimental evidences of Co/Cu(100), Co/Cu(111), Co/Cu(001) epitaxial films; ♦ (Ref. 10), ▲ (Ref. 10), and ★ (Ref. 10) denote Co_1Ni_1/Cu(100), Co_1Ni_3/Cu(100), Co_1Ni_9/Cu(100) epitaxial thin films, respectively. Inset: the dashed, the short dotted, the dotted, the solid, and the dash-dotted lines denote Eqs. (1a), (1b), (3), (4), (14), and (15), respectively. The parameters utilized in the calculations for Co are listed as: $\xi=0.396$ nm in Eq. (1b) (Ref. 36), $c=1/2$ and $S_b=117.62$ $J\cdot g\text{-atom}^{-1}\cdot K^{-1}$ in Eq. (4) (Ref. 38), and $D'=0.180$ nm, $\xi_0=0.324$ nm, and $\lambda=1.02$ in Eq. (15), respectively.

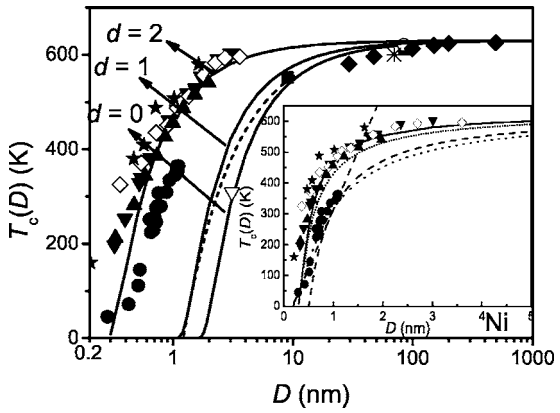

FIG. 3. Comparisons of $T_c(D)$ function between the model predictions in terms of Eq. (14) and available experimental evidences for Ni nanoparticles ($d=0$), nanorods ($d=1$), and thin films ($d=2$), respectively, where the parameters $D_0=1.4952$, 0.9968, 0.2492 nm in term of Eq. (9) with $d=0$, 1, 2, and $\alpha_s=1.811$ in light of Eq. (11) for nanoparticles and nanorods, and $\alpha_i=\alpha_s=1.811$ in terms of Eq. (13) with $J_s \approx J_i$ and $J_{\text{sub}} \approx 0$ for epitaxial films on inert substrates (Ref. 40). The prediction of Eq. (2) is shown as the short dashed with $\Delta L=0.8084$ nm in terms of Eq. (17). Other parameters used for calculations are listed in Table I. The symbols ▼,(Ref. 10), ▲ (Ref. 10), ● (Ref. 11), ★ (Ref. 12), and ◇ (Ref. 13) denote the experimental evidences of Ni/Cu(111), Ni/Cu(100), Ni/Cu(001), Ni/W(110) epitaxial films; ♦ (Ref. 18), ∗ (Ref. 19) denote Ni nanorods; and ○ (Ref. 19) ■ (Ref. 20), ▽ (Ref. 39) denote Ni nanoparticles. Inset: the dashed, the short dotted, the dotted, and the solid lines denote Eqs. (1), (3), (4), and (14), respectively. The parameters utilized in the calculations are listed as: $\xi=0.846$ nm and $\lambda=1$ in Eq. (1) (Ref. 36), $c=1/2$, and $S_b=116.22$ $J\cdot g\text{-atom}^{-1}\cdot K^{-1}$ in Eq. (4) (Ref. 38), respectively.

5), Ag(111) (Ref. 6), Ag(100) (Ref. 7) the model prediction of Eq. (14) (the solid line) shows a better agreement with the presented experimental data than that of Eqs. (1), (3), and (4) in the full size range. Although Eqs. (1) and (3) can also fit the experimental results, some adjustable parameters, such as ξ and λ in Eq. (1) and w in Eq. (3), are present. The utilization of these fitting parameters could mislead understanding of the related physical nature since the Fe/ substrate interface effect on $T_c(D)$ is taken into consideration in Eqs. (1) and (3) also through the above fitting parameters.[36–39] Namely, the fitting parameters actually consist of several factors.

It is well known that the depressed $T_c(D)$ of FM nanocrystals is induced by a reduction in the number of spin interactions at the surface in comparison with that in the interior.[36,37,39,42,43,46] The agreement between Eq. (14) and the experimental data implies that the depression of $T_c(D)$ of Fe epitaxial films on inert substrates should mainly be attributed to the effect of the free surface of nanocrystals.[36,37,39]

Similar results can be gotten in Fig. 2 and its inset for $T_c(D)$ for epitaxial Co, Co_1Ni_1, Co_1Ni_3, and Co_1Ni_9 thin films on Cu(100) (Refs. 8 and 10), Cu(111) (Ref. 10), and Cu(001) (Refs. 9 and 11) substrates. For alloys, the corresponding $T_c(\infty)$[38] and $S_m(\infty)$[42] values in Eq. (14) are roughly estimated by their algebraic sum of elements.[38] As shown in the figure, Eq. (14) corresponds to experimental measurements well. Other theoretical works, namely Eqs. (1), (3), and (4), are also plotted in the inset of the figure. Note that an additional model, a finite-size scaling relationship,[9,10] is also given in the figure shown as the dash-dotted lines, which has the following form:

$$[T_c(\infty)-T_c(D)]/T_c(D)=[(D-D')/\xi_0]^{-\lambda} \qquad (15)$$

with $T_c(D)=0$ at a finite film thickness D', and ξ_0 denoting a microscopic length characteristic of the particular system. Although Eq. (15) can also fit the experimental data,[9,10] it strictly holds only in the large size limit of D with the help of three adjustable parameters D', D_0, and λ. Since these parameters are different case by case during the fitting the experimental results when the experimental sources are different,[9,10] the physical meaning of these parameters are unclear. Other models of Eqs. (1), (3), and (4) have similar characteristics in Fig. 1, and here thus no further discussion is given.

Figure 3 shows comparisons of $T_c(D)$ functions for Ni nanocrystals with different dimensions, $d=0$ nanoparticles, $d=1$ nanorods, and $d=2$ thin films between experimental results and this model, respectively. As seen in this figure, the $T_c(D)$ function of low-dimensional Ni nanocrystals decreases

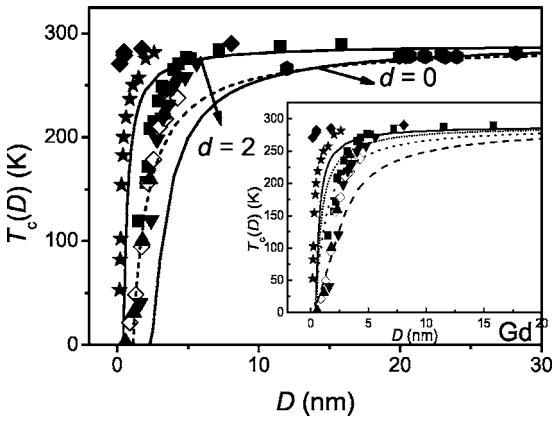

FIG. 4. Comparisons of $T_c(D)$ function between the model prediction in terms of Eq. (14) (solid lines) and available experimental results for Gd low-dimensional crystals: nanoparticles and epitaxial thin films, respectively, where the parameters $D_0=2.145$, 0.3575 nm according to Eq. (9) with $d=0$, 2, and $\alpha_s=1.508$ in terms of Eq. (11), $\alpha_i=\alpha_s=1.508$ in terms of Eq. (13) with $J_s\approx J_i$ and $J_{\text{sub}}\approx 0$ for epitaxial films on inert substrates (Ref. 40). The short dashed line denotes Eq. (2) with $\Delta L=0.7264$ nm in terms of Eq. (17). Other parameters used to calculations are listed in Table I. The symbols ■ (Ref. 14), ◆ (Ref. 14), ◇ (Ref. 15), ▼ (Ref. 16) ▲ (Ref. 16), ★ (Ref. 17) denote the experimental measurements of Gd/W(110), Gd/W, Nb/Gd, and Gd/Y(0001) epitaxial films; ⬟ (Ref. 21) denotes Gd nanoparticles. Inset: the dashed, short dotted, dotted, and solid lines denote Eqs. (1), (3), (4), and (14) for Gd epitaxial films, respectively. The parameters used in the calculations are listed as: $\xi=2.485$ nm and $\lambda=1.6$ in Eq. (1)(Ref. 36), $c=1/2$ and $S_b=101.55$ $J\cdot g\text{-atom}^{-1}\cdot K^{-1}$ in Eq. (4) (Ref. 38), respectively.

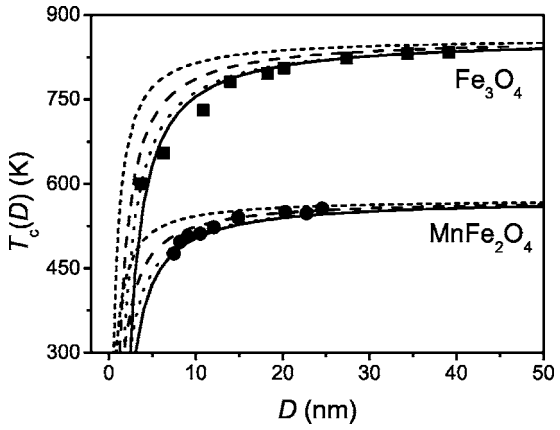

FIG. 5. Comparisons of $T_c(D)$ function between the model predictions in terms of Eq. (14) and the available experimental evidences for $MnFe_2O_4$ and Fe_3O_4 nanoparticles, where the parameters $D_0=1.338$, 1.332 nm in terms of Eq. (9) with $d=0$, and $\alpha_s=1.8458$, 1.8458 in terms of Eq. (11). The dotted, dashed, short dashed, and solid lines denote model predictions of Eqs. (2)–(4) and (14), respectively. The parameters utilized in the calculations: $\Delta L=0.7544$, 0.751 nm in Eq. (2), which is determined by Eq. (17), $c=1$ and $S_b=13R$, $13R$ $J\cdot g\text{-atom}^{-1}\cdot K^{-1}$ (Ref. 38) in Eq. (4) for $MnFe_2O_4$ and Fe_3O_4, respectively. Other parameters are listed in Table I. The symbols ● (Ref. 22) and ■ (Ref. 39) denote the experimental results of $MnFe_2O_4$ and Fe_3O_4 nanoparticles, respectively.

with D. Furthermore, the change of the $T_c(D)$ function of nanorods with D is weaker than that of nanoparticles, but stronger than that of thin films. These differences are induced by different surface/volume ratios of free nanocrystals.[36,45] Equation (14) could describe this kind of change induced by dimensions through introducing d values in Eq. (9). Since the freestanding materials have a larger surface/volume ratio, their size dependences are stronger than that of substances supported by substrates. However, this dimension effect has been neglected in Eqs. (1), (2), and (4). It is worth mentioning that, for Ni nanoparticles, the prediction according to Eq. (2) has also been presented as the short dashed line showing a good consistency with Eq. (14) and the experimental data in the large size. In addition, an enlarged figure of Ni epitaxial thin films has been shown as an inset of this figure, which presents comparisons between the model predictions of Eqs. (1), (3), (4), and (14) and experimental data for Ni films epitaxially grown on inert metallic substrates of Cu(111) (Ref. 10 and 12), Cu(100) (Ref. 10), Cu(001) (Ref. 9 and 11), and W(110) 13). As shown in the figure, Eq. (14) has similar results of Eqs. (2) and (3) for nanoparticles and thin films in the full size range, but corresponds to Eqs. (1) and (4) only in the partial size range.

Experimental $T_c(D)$ data of Gd nanoparticles[21] and epitaxial films deposited on inert metallic substrates of W(110) (Ref. 14), W (Ref. 15), Nb (Ref. 16), and Y(0001) (Ref. 17) are given in Fig. 4, which are compared with Eq. (14) where correspondence between them is found. The wide distribution of $T_c(D)$ of Gd nanocrystals indicates that $T_c(D)$ is strongly dependent on the films morphology,[17] as well as on the lattice misfit between the Gd film and the substrate.[14] For simplicity, these factors are neglected in this model. Equation (2) is shown as the short dashed line in this figure for Gd nanoparticles, which approximately corresponds to Eq. (14) and the experimental data in the large size range. In addition, Eqs. (1), (3), and (4) for Gd thin films are also present in the inset for comparisons, a scatter of the models has been illustrated as above.

In addition to the aforementioned metallic substances, $T_c(D)$ functions of compound nanocrystals such as Fe_3O_4 (Ref. 39) and $MnFe_2O_4$ (Ref. 22) nanoparticles are given in Fig. 5. As shown in the figure, the depressed $T_c(D)$ of compound nanocrystals also follows Eq. (14) as D decreases, where the prediction of Eq. (14) has better agreement with the experimental data than that of Eqs. (2)–(4) in the full size range.

Base on this idea of this work, $T_N(D)$ should have a form similar to the $T_c(D)$ function. If Eqs. (1)–(4) are extended to the Néel transition of AFM nanocrystals, the predictions of these models has also been shown in Fig. 6 for CuO nanorods[33] and nanoparticles,[30–33] and Ho[23] and NiO[28,29] thin films, respectively. Model predictions of $T_N(D)$ functions according to Eq. (14) are shown as the solid lines in this figure. As shown in this figure, the $T_N(D)$ function decreases with D for AFM nanocrystals with different dimensions, and the predictions of Eq. (14) are in better agreement with the experimental data than that of Eqs. (1)–(4) in the full size range.

Similar results for CoO thin films epitaxially grown on SiO_2 substrate[26,27] have been shown in Fig. 7. For CoO thin

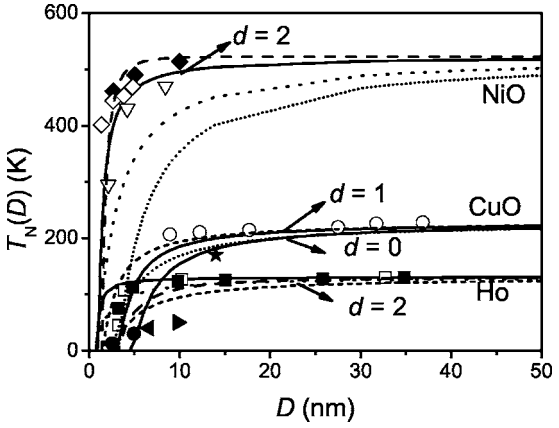

FIG. 6. Comparisons of $T_N(D)$ between the model predictions in terms of Eq. (14) and the available experimental evidences for CuO nanoparticles [○ (Ref. 30), ◀ (Ref. 31), ★ (Ref. 32), and ▶ (Ref. 33)] and nanorods [● (Ref. 33)], and Ho [■ and □ (Ref. 23] and NiO thin films [◆, ◇ (Ref. 28) and ▽(Ref. 29)], respectively. In light of the properties of magnetic exchange interaction of AFM, the nearest spacing of the parallel spin-spin coupling of AFM $h=2a$ with a being the lattice parameter since the lattice of AFM can be considered to consist of two sublattice with opposite spin direction (Ref. 48). The parameters $D_0=2.738$, 4.107 nm for CuO nanorods and nanoparticles in terms of Eq. (9) with $d=0$, 1, and $D_0=(2h)/2=h=0.7154$, 0.8420 nm for Ho and NiO thin films with $d=2$, respectively, and $\alpha_s=1.563$ for CuO in terms of Eq. (11) and $\alpha_i=\alpha_s=1.561$, 1.583 for Ho and NiO thin films in terms of Eq. (13) with $J_s\approx J_i$ and $J_{\text{sub}}\approx 0$ for epitaxial films on inert substrates. The dashed, short dashed, short dotted, and dotted lines, denote the predictions of Eqs. (1)–(4), respectively. Calculation parameters used are listed in Table II. In addition, the parameters $\xi=3.13$, 1.4 nm and $\lambda=1.58$, 2.8 in Eq. (1a) for Ho, and NiO, $\Delta L=1.541$ in Eq. (2) for CuO, $c=1/2$, $S_b=6.511$, $13R$, and $13R$ $J\cdot g\text{-atom}^{-1}\cdot\text{K}^{-1}$ in Eq. (4) for Ho, NiO, and CuO (Ref. 38), respectively.

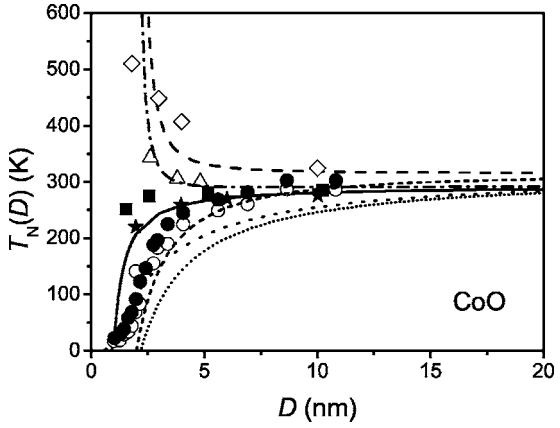

FIG. 7. Comparisons of $T_N(D)$ between the model predictions in terms of Eq. (14) (solid line) and available experimental evidences for CoO thin films epitaxially grown on SiO_2 substrates [● and ○ (Ref. 26 ■ and ★ Ref. 27)], where the parameters $D_0=(2h)/2=h=0.8520$ nm in terms of Eq. (9) with $d=2$, and $\alpha_i=1.544$ according to Eq. (13) with $J_s\approx J_i$, $J_{\text{sub}}\approx 0$ and $\alpha_s=1.544$ in terms of Eq. (11). Calculation parameters used are listed in Table II. The short dashed, short dotted, and dotted lines denote the predictions according to Eqs. (1), (3), and (4), respectively, in which the parameters $\xi=2.1$ nm and $\lambda=1.55$ (Ref. 26), $c=1/2$ and $S_b=13R$ (Ref. 38). The dashed and dashed dotted lines, respectively, denote the model predictions in terms of Eq. (14) for CoO supported by Fe_3O_4 and NiO substrates with the parameter $\alpha_i=0.4139$ and 0.5544 in terms of Eq. (13) with $\alpha_s J_s/(J_s+J_{\text{sub}})\approx\alpha_s T_c(\infty)/[T_c(\infty)+T_{c,\text{sub}}(\infty)]$, which is achieved based on the mean-field approximation, $J_s\propto T_c(\infty)$ and $J_{\text{sub}}\propto T_{c,\text{sub}}(\infty)$ or $J_s\propto T_N(\infty)$ and $J_{\text{sub}}\propto T_{N,\text{sub}}(\infty)$ (Ref. 45). The symbols △ (Ref. 28) and ◇ (Ref. 34) denote the experimental results of CoO thin films supported by Fe_3O_4 and NiO substrates, respectively.

films supported by Fe_3O_4 and NiO substrates, there exist, however, strong exchange couplings at the CoO/Fe_3O_4 or CoO/NiO interface where the thermal vibration of the interface atoms is suppressed and much higher energy is required to disorder the ordering force.[28,34] Therefore, $T_N(D)$ increases as D decreases. The predicted results of Eq. (14) with consideration on the substrates[34,49] are qualitatively consistent with experimental evidence. Note that other models have not been considered in this kind of case.[28,34,36,38,39] Although the free surface of such CoO film still has a tendency to lower the $T_N(D)$ value of the films, the total effect of the free surface and the interface leads to a drop in the total energy of the film, and thus the increase of the $T_N(D)$ function with decreasing D. Furthermore, the stronger the interaction at the interface is, the more the $T_N(D)$ function increases.[28,34] Thus, different substrates lead to distinct values of $T_N(D)$ and $T_N(\infty)$ of CoO.[26–28,34] For the sake of simplicity, the exchange bias effect from the FM/AFM interface, existence of easy and hard axes, and magnetocrystalline anisotropy are neglected.

Note that the above results differ from the experimental result of Fe/Cr(100), where $T_N(D)$ decreases with dropping D,[50] which could be induced by spin-frustration effects in the vicinity of the rough Fe/Cr interfaces where the interfacial exchange energy can be minimized only locally and frustration of the interfacial spins occurs since Fe and Cr have magnetical long-range order.[50]

In terms of this model, it is easy to understand that if one needs to disorder the spin-spin interaction by applying a thermal stimulus, one has to provide sufficient energy to lose all bonds of atoms and to promote the atomic vibration.[39] At the Curie transition of FM or Néel transition of AFM, the thermal vibrational energy of atoms of low-dimensional material

TABLE II. The parameters utilized in the calculations of Eq. (14) about AFM materials. $T_N(\infty)$ is in K, $S_m(\infty)$ in $J\cdot g\text{-atom}^{-1}\cdot\text{K}^{-1}$, and h is in nm.

	$T_N(\infty)$	$S_m(\infty)$[a]	h
Ho	131.2[23]	6.999[51]	0.7154[51]
NiO	523[28]	7.271	0.8420[28]
CoO	315[26,27]/293[28]	6.789	0.8520[28,34]
CuO	229[33]	7.016	0.6845[33]

[a] $S_m(\infty)$ of metallic oxides are given as $S_{m,MO}(\infty)=[S_{m,M}(\infty)+S_{m,O}(\infty)]/2$ as a first approximation since no experimental data are found, where the subscripts M and O denote the metal and oxygen atoms, respectively.

is required to disorder E_{exc}.[36,45,46] As pointed out in the experimental observations for free nanocrystals (nanoparticles, nanorods, thin films) or epitaxial thin films on inert substrates,[46,47] there exist different degrees of spin-spin interactions between inner and surface atoms because of the reduction in the number of spin interactions at the surface,[36] which leads to an increase of lattice vibration.[37,39,42,43,46] For thin films with strong interaction coupling at the film/substrate interface, however, the vibration of atoms at this interface is depressed. Thus, as D is reduced, the total energy, or the thermal vibration energy to disorder the FM or AFM ordering state of the nanocrystals, could increase or decrease depending on the interface states. So does the $T_c(D)$ or $T_N(D)$ function.

As mentioned previously, the depressed order temperature of FM or AFM free nanocrystals is mainly induced by the free surface of nanocrystals. When d is different, the surface/volume ratio $A/V=6/D$, $4/D$, and $2/D$ as $d=0$, 1, 2, respectively. Thus, $T_c(D)$ or $T_N(D)$ function with different d values is changed in a different degree even though their D are the same. As shown in Figs. 3–6 at the same D value, the decrease of $T_c(D)$ or $T_N(D)$ function is smaller as d varies from 0 to 2.

As shown in these figures, complicated $T_c(D)$ and $T_N(D)$ functions are still analyzed and predicted by this simple and unified model as long as the surface or interface conditions of the low-dimensional crystals and relative thermodynamic parameters are known.

Considering the mathematical relationship of $\exp(-x) \approx 1-x$ when x is small enough as a first order approximation, under the condition that $D \gg D_0$, Eq. (14) can be simplified as follows:

$$T_c(D)/T_c(\infty) = T_N(D)/T_N(\infty) \approx 1 - (\alpha_s + \alpha_i - 2)D_0/(2D). \quad (16)$$

Equation (16) indicates that the most important size effect for low dimensional FM and AFM nanocrystals is still related with the surface/volume ratio, or $1/D$, and suggests a progressively increasing role of the surface layer with decreasing D. However, as D approaches D_0, Eq. (16) gives an error in comparison with Eq. (14). This is because as D decreases to a size being comparable with atomic diameter, transition temperature is also contributed by energetic changes of internal atoms.

Comparing Eq. (16) with the scaling law of Eq. (1a) for thin films with $D > \xi$, $T_c(D)$ follows a power law curve with $\lambda=1$ (Ref. 36). Thus, Eq. (1a) can be rewritten as $T_c(D)/T_c(\infty)=T_N(D)/T_N(\infty)=1-[(\xi+r_0)/(2D)]$ (Ref. 36). Associated with this relationship and Eq. (16), $\xi=(\alpha_s+\alpha_i-2)D_0-r_0$. For Fe, Co, Ni thin films, $\xi=0.4048$, 0.5531, 0.6322 nm, respectively, which are approximately consistent with experimental and theoretical values of 0.4583, 0.3962, 0.7048 (Ref. 36).

It is evident that Eq. (16) has a similar form of Eq. (2) for nanoparticles. Combining Eqs. (2) and (16),

$$\Delta L \approx 2(\alpha_s - 1)D_0/3, \quad (17)$$

which indicates that ΔL is related to two parameters, S_{vib} and h. Substituting these parameters into Eq. (17), $\Delta L=0.8084$, 0.9692, 0.7521, 0.7512, and 1.541 nm for Ni, Gd, $MnFe_2O_4$, Fe_3O_4, and CuO nanoparticles, respectively. With the ΔL values, the predictions of Eq. (2) are shown in Figs. 3–6 as the short dashed lines. The results of Eq. (2) are in agreement with the experimental data when D is large enough where $\Delta L \approx 3h$. Thus, when D is larger than several nanometers, Eq. (2) can be rewritten as follows:

$$T_c(D)/T_c(\infty) = T_N(D)/T_N(\infty) \approx 1 - (9h)/(2D). \quad (18)$$

Equation (18) becomes a pure geometrical equation and emphasizes the surface contribution on the $T_c(D)$ function.

In light of Eqs. (3) and (16),

$$\sum_{i\leqslant 3} q_i(z_{ib}q_i^{-w} - 1) \approx -(\alpha_s + \alpha_i - 2). \quad (19)$$

Obviously, w is a function of materials, as well as interface conditions, which has been taken as an adjustable material constant in Eq. (3). According to Eq. (19), $\Sigma_{i\leqslant 3}q_i(z_{ib}q_i^{-w} - 1)=0.0421$ for the case of CoO epitaxial films on Fe_3O_4 substrates. With this value, the $T_N(D)$ function of Eq. (3) is predicted to increase as D is reduced, which is qualitatively consistent with the experimental evidence.

Compared with the previous models,[36–39,45,46] this unified model without any adjustable parameter can be utilized to predict the effects of dimension and interface on the $T_c(D)$ or $T_N(D)$ function through introducing the parameter D_0 and α, respectively. When $0<\alpha<1$, $T_c(D)$ or $T_N(D)$ increases with decreasing D, while the contrary occurs when $\alpha>1$, which is determined by the common effects of both the surface and film/substrate interface with different interface interaction strengths. Furthermore, when Eq. (14) is reasonable, the adjustable parameters which appeared in Eqs. (1)–(3) could be quantitatively determined and a more exact physical meaning of these parameters may be found.

IV. CONCLUSION

In summary, size, dimension, and interface effects on the $T_c(D)$ and $T_N(D)$ functions of low-dimensional FM and AFM have been modeled. In terms of this model, $T_c(D)$ and $T_N(D)$ functions decrease or increase with dropping D and d, which is determined by the interfacial conditions. When there is no or a weak interaction on the interface, these functions decrease with D; while when the interface interaction is strong, $T_c(D)$ and $T_N(D)$ functions increase as D is reduced. The predicted results are in agreement with available experimental measurements of Fe, Co, Ni, Gd, Ho, Co_1Ni_1, Co_1Ni_3, Co_1Ni_9, Fe_3O_4, $MnFe_2O_4$, CoO, NiO, and CuO low-dimensional nanocrystals.

ACKNOWLEDGMENT

Financial support by National Key Basic Research and Development Program (Grant No. 2004CB619301), NNSFC (Grant No. 50525204), and by the "985 Project" of Jilin University are acknowledged.

*Corresponding author. Email address: jiangq@jlu.edu.cn

[1] D. D. Fong, G. B. Stephenson, S. K. Streiffer, J. A. Eastman, O. Auciello, P. H. Fuoss, and C. Thompson, Science **304**, 1650 (2004).
[2] E. L. Lee, P. E. Bolduc, and C. E. Violet, Phys. Rev. Lett. **13**, 800 (1964).
[3] M. Stampanoni, A. Vaterlaus, M. Aeschlimann, and F. Meier, Phys. Rev. Lett. **59**, 2483 (1987).
[4] W. Dürr, M. Taborelli, O. Paul, R. Germar, W. Gudat, D. Pescia, and M. Landolt, Phys. Rev. Lett. **62**, 206 (1989).
[5] C. Liu and S. D. Bader, J. Appl. Phys. **67**, 5758 (1990).
[6] Z. Q. Qiu, J. Pearson, and S. D. Bader, Phys. Rev. Lett. **67**, 1646 (1991).
[7] Z. Q. Qiu, J. Pearson, and S. D. Bader, Phys. Rev. Lett. **70**, 1006 (1993).
[8] C. M. Schneider, P. Bressler, P. Schuster, J. Kirschner, J. J. de Miguel, and R. Miranda, Phys. Rev. Lett. **64**, 1059 (1990).
[9] F. Huang, G. J. Mankey, M. T. Kief, and R. F. Willis, J. Appl. Phys. **73**, 6760 (1993).
[10] F. Huang, M. T. Kief, G. J. Mankey, and R. F. Willis, Phys. Rev. B **49**, 3962 (1994).
[11] F. May, P. Srivastava, M. Farle, U. Bovensiepen, H. Wende, R. Chauvistré, and K. Baberschke, J. Magn. Magn. Mater. **177–181**, 1220 (1998).
[12] C. A. Ballentine, R. L. Fink, J. Araya-Pochet, and J. L. Erskine, Phys. Rev. B **41**, 2631 (1990).
[13] Y. Li and K. Baberschke, Phys. Rev. Lett. **68**, 1208 (1992).
[14] M. Farle, K. Baberschke, U. Stetter, A. Aspelmeier, and F. Gerhardter, Phys. Rev. B **47**, 11571 (1993).
[15] J. S. Jiang and C. L. Chien, J. Appl. Phys. **79**, 5615 (1996).
[16] J. S. Jiang, D. Davidović, D. H. Reich, and C. L. Chien, Phys. Rev. Lett. **74**, 314 (1995).
[17] M. Gajdzik, T. Trappmann, C. Sürgers, and H. V. Löhneysen, Phys. Rev. B **57**, 3525 (1998).
[18] L. Sun, P. C. Searon, and C. L. Chien, Phys. Rev. B **61**, R6463 (2000).
[19] X. F. Cui, M. Zhao, and Q. Jiang, Thin Solid Films **472**, 328 (2005).
[20] Y. W. Du, M. X. Xu, J. Wu, Y. B. Shi, H. X. Lu, and R. H. Xue, J. Appl. Phys. **70**, 5903 (1991).
[21] D. Michels, C. E. Krill III, and R. Birringer, J. Magn. Magn. Mater. **250**, 203 (2002).
[22] Z. X. Tang, C. M. Sorensen, K. J. Klabunde, and G. C. Hadjipanayis, Phys. Rev. Lett. **67**, 3602 (1991).
[23] E. Weschke, H. Ott, E. Schierle, C. Schüssler-Langehenine, D. V. Vyalikh, G. Kaindl, V. Leiner, M. Ay, T. Schmitte, H. Zabel, and P. J. Jensen, Phys. Rev. Lett. **93**, 157204 (2004).
[24] E. E. Fullerton, S. Adenwalla, G. P. Felcher, K. T. Riggs, C. H. Sowers, S. D. Bader, and J. L. Robertson, Physica B **221**, 370 (1996).
[25] E. E. Fullerton, S. D. Bader, and J. L. Robertson, Phys. Rev. Lett. **77**, 1382 (1996).
[26] T. Ambrose and C. L. Chien, Phys. Rev. Lett. **76**, 1743 (1996).
[27] Y. J. Tang, D. J. Smith, B. L. Zink, F. Hellman, and A. E. Berkowitz, Phys. Rev. B **67**, 054408 (2003).
[28] E. N. Abarra, K. Takano, F. Hellman, and A. E. Berkowitz, Phys. Rev. Lett. **77**, 3451 (1996).
[29] D. Alders, L. H. Tjeng, F. C. Voogt, T. Hibma, G. A. Sawatzky, C. T. Chen, J. Vogel, M. Sacchi, and S. Iacobucci, Phys. Rev. B **57**, 11623 (1998).
[30] A. Punnoose, H. Magnone, M. S. Seehra, and J. Bonevich, Phys. Rev. B **64**, 174420 (2001).
[31] A. Punnoose and M. S. Seehra, J. Appl. Phys. **91**, 7766 (2002).
[32] S. J. Stewart, M. Multigner, J. F. Marco, F. J. Berry, A. Hemando, and J. M. Gonzalez, Solid State Commun. **130**, 247 (2004).
[33] X. G. Zheng, C. N. Xu, K. Nishikubo, K. Nishiyama, W. Higemoto, W. J. Moon, E. Tanaka, and E. S. Otabe, Phys. Rev. B **72**, 014464 (2005).
[34] P. J. van der Zaag, Y. Ijiri, J. A. Borchers, L. F. Feiner, R. M. Wolf, J. M. Gaines, R. W. Erwin, and M. A. Verheijen, Phys. Rev. Lett. **84**, 6102 (2000).
[35] M. E. Fisher and M. N. Barber, Phys. Rev. Lett. **28**, 1516 (1972).
[36] R. J. Zhang and R. F. Willis, Phys. Rev. Lett. **86**, 2665 (2001).
[37] V. I. Nikolaev and A. M. Shipilin, Phys. Solid State **45**, 1079 (2003).
[38] C. C. Yang and Q. Jiang, Acta Mater. **53**, 3305 (2005).
[39] C. Q. Sun, W. H. Zhong, S. Li, B. K. Tay, H. L. Bi, and E. Y. Jiang, J. Phys. Chem. B **108**, 1080 (2004).
[40] F. Aguilera-Granja and J. L. Morán-López, Solid State Commun. **74**, 155 (1990).
[41] J. G. Dash, Rev. Mod. Phys. **71**, 1737 (1999).
[42] X. Y. Lang and Q. Jiang, Solid State Commun. **134**, 797 (2005).
[43] Q. Jiang, H. Y. Tong, D. T. Hsu, K. Okuyama, and F. G. Shi, Thin Solid Films **312**, 357 (1998).
[44] Q. Jiang and X. Y. Lang, Macromol. Rapid Commun. **25**, 825 (2004).
[45] W. H. Zhong, C. Q. Sun, B. K. Tay, S. Li, H. L. Bai, and E. Y. Jiang, J. Phys.: Condens. Matter **14**, L399 (2002).
[46] W. H. Zhong, C. Q. Sun, S. Li, H. L. Bai, and E. Y. Jiang, Acta Mater. **53**, 3207 (2005).
[47] A. Hernando, J. Phys.: Condens. Matter **11**, 9455 (1999).
[48] J. H. van Vleck, Rev. Mod. Phys. **17**, 27 (1945).
[49] J. Unguris, R. J. Celotta, and D. T. Pierce, Phys. Rev. Lett. **69**, 1125 (1992).
[50] E. E. Fullerton, K. T. Riggs, C. H. Sowers, S. D. Bader, and A. Berger, Phys. Rev. Lett. **75**, 330 (1995).
[51] http://www.webelements.com/